

1 **Patient-Specific 3D Scanned and 3D Printed Antimicrobial Polycaprolactone Wound**
2 **Dressings**

3

4

5 Zaid Muwaffak Hassan ^a, Alvaro Goyanes ^b, Vivienne Clark ^a, Abdul W. Basit ^{a,b} Stephen T. Hilton ^a,
6 Simon Gaisford ^{a,b}

7 ^a UCL School of Pharmacy, University College London, 29-39 Brunswick Square, London, WC1N 1AX,
8 UK

9 ^b FabRx Ltd., 3 Romney Road, Ashford, Kent TN24 0RW, UK

10

11 **Corresponding authors:**

12 Stephen Hilton

13 Simon Gaisford

14 s.hilton@ucl.ac.uk

15 s.gaisford@ucl.ac.uk

16

17

18 **Abstract**

19 The increasing prevalence of wound infections caused by antibiotic resistant bacteria is an urgent
20 challenge facing modern medicine. To address this issue the expedient use of antimicrobial metals
21 such as zinc, copper and silver were incorporated into an FDA-approved polymer (polycaprolactone -
22 PCL) to produce filaments for 3D printing. These metals have broad-spectrum antimicrobial
23 properties, and moreover, copper and zinc can enhance the wound healing process. 3D scanning
24 was used to construct 3D models of a nose and ear to provide the opportunity to customize shape
25 and size of a wound dressing to an individual patient. Hot melt extrusion was used to extrude pellets
26 obtained by vacuum-drying of solutions of PCL and the different metals in order to manufacture
27 metal-homogeneously-loaded filaments. Wound dressings with different shapes were produced with
28 the filaments containing different concentrations of metals. Release of the metals from the dressings
29 was determined by inductively coupled plasma atomic emission spectroscopy. All the different metal
30 dressings show fast release (up to 24 h) followed by slow release (up to 72 h). The antibacterial
31 efficacy of the wound dressings was tested using a thermal activity monitor system, revealing that
32 silver and copper wound dressings had the most potent bactericidal properties. This study shows
33 that 3D scanning and 3D printing, which are becoming simpler and more affordable, have the
34 potential to offer solutions to produce personalised wound dressings.

35

36

37

38 **Keywords:**

39 3D printing

40 3D scanning

41 Wound dressings

42 Polycaprolactone

43 Additive manufacturing

44 Personalised medicine

45

46

47 **1 Introduction**

48 The skin is the largest organ in the body, functioning as a sensory system, regulating both
49 temperature and moisture transmission and acts as a physical barrier against the external
50 environment. When a wound occurs, due to trauma or disease, the barrier becomes compromised.
51 This can increase the susceptibility of the wound site to microbial infections originating from
52 endogenous sources, such as surrounding skin and mucous membranes, or from exogenous sources,
53 such as those introduced by injury or from the local environment (Landis, 2008). The introduced
54 microorganism may overcome the host's defences and invade into deeper tissues, progressing to a
55 more severe infection, thus causing further damage and delaying healing of the wound (Siddiqui and
56 Bernstein, 2010).

57 A wound may require the application of an external dressing to temporarily compensate for the
58 damaged barrier and to allow healing to initiate and progress. A wound dressing isolates the injury
59 site from the external environment, and provides an optimal environment for the wound to heal by
60 promoting haemostasis and limiting tissue oedema through external compression (Zahedi et al.,
61 2010). Wound dressings, traditionally used to protect the wound from contamination, can be used
62 as platforms to deliver actives to wound sites. The use of solid wound dressings is preferred to the
63 use of topical bioactive agents in the form of solutions, creams, and ointments in the case of
64 exudative wounds for drug delivery to the wound as they provide better exudate management and
65 prolonged residence at the wound site. These dressings are potentially useful in the treatment of
66 local infections being beneficial to achieve increased local concentrations of antibiotics while
67 avoiding systemic treatment, thus reducing patient exposure to an excess of drug beyond that
68 required at the wound site (Boateng and Catanzano, 2015).

69 Due to the alarming increase of multi-drug resistance bacteria worldwide, caused by the over-use
70 and miss-use of antibiotics, the application of broad-spectrum antimicrobial agents such as metal
71 ions is an attractive target. Having been used historically for their antimicrobial properties (Lemire et
72 al., 2013; Tenaud et al., 2009), the use of inorganic antimicrobial metals in the fight against
73 infections is of high importance due to the fact that they act on multiple bacterial pathways, which
74 makes it difficult for the bacteria to develop resistance against them (Huh and Kwon, 2011). Silver is
75 probably the most commonly used metal, but zinc and copper, two of the essential trace elements in
76 the human body, are also known to play an integral part in the wound healing process.

77 Silver ions have been shown to bind to various bacterial cell membrane proteins to cause cell lysis,
78 and can be transported into bacterial cells, where silver ions disrupt the cell wall to interfere with
79 energy production, enzyme function, cell replication and ultimately cell death (Chopra, 2007; Fong
80 and Wood, 2006; Jain et al., 2009). There remains a concern in relation to the toxicity of silver to
81 humans, however, most frequent side effects including local skin irritation, discolouration or staining
82 which are harmless and usually reversible (Cutting et al., 2007). Copper ions function by altering
83 proteins and inhibiting their biological activity, membrane lipid peroxidation, and plasma membrane
84 permeabilization (Borkow and Gabbay, 2005; Gabbay et al., 2006). Copper can improve the healing
85 process as it plays a key role in the enhancement of angiogenesis, via induction of vascular
86 endothelial growth factor (VEGF), up-regulating the activity of copper-dependent enzymes, cell
87 proliferation and re-epithelisation (Liu et al., 2009). It is suggested that the mode of action of ZnO is
88 due to the disruption of bacterial cell membranes, and zinc is involved in several transcription
89 factors and enzyme systems, stimulates the proliferation of epidermal cells, and increases collagen
90 synthesis. Topical zinc can improve the healing of wounds especially in patients with zinc deficiency
91 (Lemire et al., 2013), which can be a result of hereditary causes (Lansdown et al., 2007).

92 Wound dressings are usually prepared from absorbent, cross-linked polymer networks. One
93 potential polymer is polycaprolactone (PCL), a semi-crystalline polyester that is biodegradable and
94 biocompatible. These properties have led to the approval of several PCL drug-delivery devices and
95 implants by the FDA (Salgado et al., 2012). It has a slow rate of degradation *in-vivo* compared with
96 other biodegradable polyesters, a property that can be exploited in the manufacture of controlled
97 release formulations (Li et al., 2014). PCL has been widely investigated in wound and burn dressings
98 (Boateng et al., 2008; Ng et al., 2007), tissue engineering (Kweon et al., 2003), scaffold
99 manufacturing (Kamath et al., 2014) and drug targeting (Freiberg and Zhu, 2004).

100 Three-dimensional printing (3DP) is a recently developed technology with numerous possibilities for
101 the manufacture of medical devices. 3DP is an additive manufacturing process that allows the
102 fabrication of three dimensional solid objects of virtually any shape. Of the several types of 3D
103 printing, fused deposition modelling (FDM) has been most widely used for medical devices as it is
104 simple, cost effective and extrudes polymer strands (Goyanes et al., 2016a; Yu et al., 2008). The
105 printer feedstock is a thermoplastic filament that is heated to its softening point and then extruded
106 through a print-head (driven by an X – Y orientation system) layer by layer over a build plate. The
107 build plate is then lowered to a predetermined height and the process is repeated until the 3D
108 object has been constructed. FDM 3DP has been used in various fields, such as tissue engineering,
109 scaffold manufacturing (Fielding et al., 2012), and to produce oral drug delivery formulations
110 (Goyanes et al., 2014; Goyanes et al., 2015a; Goyanes et al., 2016b; Goyanes et al., 2015b; Melocchi
111 et al., 2015; Pietrzak et al., 2015). The ‘instructions’ for the 3D printer on how to build the object
112 comes from the printer’s software that slices the source digital file into layers that form the
113 instructions for the 3D printer. This digital file can be created using computer-aided design software,
114 to construct a new 3D object, or with the use of 3D scanning, to copy an existing object. 3D scanning
115 is a non-contact, non-destructive technology that digitally captures the shape of physical objects
116 with a 3D scanner using laser light that collects distance information from surfaces. This information
117 is then used to create ‘point clouds’ of data from the surface of the object. Hence, 3D laser scanning
118 is a way to capture a physical object’s exact size and shape to construct a 3D model (Koch, 2012).
119 The proof of concept of combining 3D printing and 3D scanning for the manufacture of antiacne
120 masks/patches has been previously reported (Goyanes et al., 2016a), whereas the use of FDM
121 printing showed high drug degradation due to the heating process while printing.

122 The combination of 3D printing and 3D scanning could possibly revolutionise patient care by
123 allowing custom-manufacture of devices for individual patients and it is the exploration of this
124 concept, applied specifically to wound dressings, that is the focus of this work. Hot melt extrusion
125 was used to incorporate metal ions into a PCL filament and the 3D printer was used to fabricate
126 dressings against scanned templates of a target wound. The antimicrobial efficacy of the dressings
127 was also assessed using an *in-vitro* assay.

128

129 **2 Materials and Methods**

130 **2.1 Materials**

131 PCL pellets ((C₆H₁₀O₂)_n, Mw ~ 80,000) and silver nitrate (AgNO₃) were purchased from Sigma-
132 Aldrich, UK. Copper sulphate (II) pentahydrate (CuSO₄·5H₂O) was purchased from VWR chemicals,
133 Belgium. Zinc oxide (ZnO) was purchased from Alfa Aesar, USA. The test organism *Staphylococcus*
134 *aureus* (NCIMB 9518) was purchased from Fisher Scientific, UK. Nutrient broth (CM0001) was
135 purchased from Thermo Scientific, UK.

136

137 2.2 Methods

138 2.2.1 Preparation of metal loaded filaments

139 - Silver-loaded filament (10% loading w/w):

140 AgNO₃ (3 g) was dissolved in 10 mL of deionized water using a magnetic stirrer. Tetrahydrofuran
141 (THF, 200 mL) was added to the silver solution under stirring. Finally, 27g of PCL pellets was then
142 added to the solution and the mixture was stirred at 40 °C until complete dissolution of PCL. The
143 solvents were removed with a rotary evaporator under reduced pressure at 40 °C for 2 h followed by
144 high-vacuum drying for 1h. The dried material (AgNO₃ homogeneously distributed in the PCL) was
145 chopped into pellets and extruded with Filabot filament hot-melt extruder (Filabot Inc, USA) with a
146 single screw and a 1.75 mm nozzle head. The extrusion temperature was 80 °C.

147

148 - Copper-loaded filament (10 and 25% loading w/w):

149 CuSO₄·5H₂O (3g or 7.5g for 10% or 25% loading respectively) was dissolved in 100mL methanol using
150 a magnetic stirrer. PCL pellets (27 g or 22.5 g for 10% or 25% copper loading respectively) was then
151 added to the copper solution, followed by 100mL dichloromethane (DCM) and the mixture was
152 stirred at 40°C until complete dissolution of PCL. A rotary evaporator (under reduced pressure) was
153 used to evaporate the solvents at 40 °C for 3 h followed by high-vacuum drying for 1 h. The dried
154 material (CuSO₄ homogeneously distributed in the PCL) was chopped into pellets and extruded with
155 Filabot filament hot-melt extruder (Filabot Inc, USA) with a single screw and a 1.75mm nozzle head.
156 The extrusion temperature was 60°C.

157

158 - Zinc-loaded filament (10 and 25% loading w/w):

159 ZnO (3g or 7.5g for 10% or 25% zinc loading respectively) was dissolved in 100 mL ethanol using a
160 magnetic stirrer. PCL pellets (27g or 22.5g for 10% or 25% copper loading respectively) was added
161 followed by 100 mL DCM and the mixture was stirred at 40°C until complete dissolution of PCL. The
162 solvents were removed using a rotary evaporator at 40 °C for 3 h followed by one hour high-vacuum
163 drying. The dried material (ZnO homogeneously distributed in the PCL) was chopped into pellets and
164 extruded with Filabot filament hot-melt extruder (Filabot Inc, USA) with a single screw and a
165 1.75mm nozzle head. The extrusion temperature was 75°C.

166

167 For all the filaments prepared the diameter of the filament was checked using a digital calliper
168 throughout the extrusion process, since it is important to get a consistent filament diameter within
169 an acceptable range for the 3D printer.

170

171 2.2.2 3D Scanning

172 3D scans were captured with a Sense 3D Scanner (3D Systems, USA). It functions by capture of the
173 surface data of a physical object reflected light from a laser. In this work, scans were captured of a
174 nose and ear, because 3D printed dressings of these body parts can dress anatomically complex
175 areas compared to conventional flat dressing, what would provide more comfort to the patient. The
176 settings used were high resolution, with object recognition enabled, colour scanning and landscape
177 orientation. The person being scanned was in a setting position, while the person holding the 3D
178 scanner was rotating 360° around the subject while maintaining about 40 cm distance to the
179 subject. These 3D scans were cut, optimized for 3D printing and templates were made using
180 Autodesk Meshmixer 10.8.

181 2.2.3 3D Printing

182 A MakerBot Replicator 2X Desktop 3D printer (MakerBot Inc., USA) was used to print wound
183 dressings shaped to match the nose and ear scans, in addition to square dressings (20 x 20 x 1 mm)
184 for antimicrobial studies and circular dressings (10 mm diameter x 1 mm thickness) for dissolution
185 testing. The templates for the square and circular dressings were created using Tinkercad (Autodesk)
186 – a browser-based 3D design and modelling tool.

187

188 The nozzle head was cleaned (for 20 – 25 s) prior to printing the metal-loaded filaments, and
189 between prints containing different metal ions or different concentrations, by extruding plain PCL
190 filament. The settings of the printer, which will ultimately determine how the 3DP dressings will turn
191 out, were selected based on preliminary results with the metal loaded filaments. All the dressings
192 were printed at an extrusion temperature of 170 °C, high resolution (0.1 mm layer height), with two
193 shells, 100% infill and speed while extruding and while travelling was set to 50 mm/s. A raft and
194 support were used for the printing of the nose and ear dressings, while no support or raft was used
195 for the printing of the flat dressings printed for analytical purposes.

196

197 **2.2.4 Thermal characterisation of metal-loaded filaments and dressings**

198 Differential scanning calorimetry (DSC): Measurements of the metal loaded filaments and the 3D
199 printed dressings were performed using a TA Q2000 DSC (TA Instruments LLC, USA), calibrated with
200 indium ($T_m = 156.6\text{ °C}$, $\Delta H_f = 28.71\text{ J/g}$). Nitrogen gas was used as a purge with a flow rate of 50
201 mL/min. Tzero hermetic pans with lids were used for all samples, with an average sample weight of
202 7-9 mg. Samples were cooled to -80 °C then heated to 200 °C at a heating rate of 10 °C/min.

203

204 Thermogravimetric analysis (TGA): TGA analysis was performed with TA Discovery TGA (TA
205 Instruments LLC, USA) with nitrogen as purge (flow rate = 25 mL/min). Open aluminium pans were
206 used, and samples were heated from room temperature ($15 \pm 0.5\text{ °C}$) to 200 °C at 10 °C/min.

207

208 **2.2.5 Scanning electron microscopy (SEM)**

209 Surface and cross-section images of the filaments were taken using JSM-840A Scanning Microscope,
210 JEOL GmbH, Germany. The voltage and working distance were set at 5 kV and 50 mm, respectively.
211 Filament samples were placed on double-sided carbon tape, mounted on stubs and sputter coated
212 using a Polaron E5000 machine with Au/Pd. Samples were coated for 1 minute prior to imaging.

213

214

215

216 **2.2.6 Fourier transform infrared (FTIR) spectroscopy**

217 FTIR spectra of Ag, Cu and Zn powder, filaments and dressings were acquired using Bruker ALPHA
218 Platinum FT-IR spectrometer (USA) to determine if Ag, Cu or Zn form any bonding with the
219 polycaprolactone matrix. Spectra were acquired at 4000 cm^{-1} to 400 cm^{-1} and a resolution of 2 cm^{-1} .

220

221 **2.2.7 Dissolution testing of wound dressings**

222 For each assay the dressing was placed into a sterile 10 mL vial with agitation in the dissolution
223 medium (10 mL of 0.1 M phosphate buffer – pH 7.4). The vials were capped and incubated in a
224 thermostated bath at 37 °C for three days. At regular intervals (0, 6, 12, 18, 24, 36, 48, 60 and 72 h),
225 1 mL aliquots were sampled from each vial and replaced with an equal amount of phosphate buffer.
226 The samples were then diluted to 5 mL with 96% (w/w) nitric acid (to digest any dissolved polymer
227 matrix), stirred at room temperature for 1 h, then 1 mL was taken from that solution and diluted
228 further to 20 mL with phosphate buffer.

229 Analysis of the samples was performed with Inductively Coupled Plasma Atomic Emission
230 Spectroscopy (ICP-AES) using an Axial Varian 720-ES, with argon as a purge gas. Ag was analysed at
231 wavelength 328.068 nm, Cu at 327.395 nm and Zn at 213.857 nm. A second wavelength (338.289 nm
232 for Ag, 324.754 nm for Cu and 202.548 nm for Zn) was used to confirm the reproducibility of the
233 results. Each dressing was tested in triplicate and the mean value determined.

234

235 **2.2.8 Antibacterial efficacy of wound dressings**

236 Antibacterial efficacy of wound dressings was tested against *S. aureus* which is a common bacterium
237 to causes skin infections. *S. aureus*, stored in 1 mL aliquots at -80 °C in 15% w/v glycerol, was
238 defrosted at 37 °C and used to inoculate nutrient broth, which was incubated overnight aerobically
239 at 37 °C. Bacteria were harvested from the broth by centrifugation at 3000 g for 10 min and washed
240 in phosphate buffered saline (PBS) (Fisher Scientific, UK) three times. The resulting bacterial
241 suspension was adjusted to a 0.5 McFarland standard using PBS to standardize the cell numbers to
242 approximately 1×10^8 cfu/mL. This was verified with serial dilution and spread plating.

243

244 Dressing samples (plain PCL, Ag-PCL, Cu-PCL, and Zn-PCL) printed with identical settings (see 3D
245 printing above) were cut to the required weights (10, 20, 25, 30, 40, 50, 75 and 100 mg) immediately
246 prior to use and inserted into a sterile 3 ml calorimetric ampoule (Hichrom, UK). Nutrient broth
247 (2.97 mL) was added to the ampoule, followed by inoculation with the bacterial suspension (30 µL).
248 The ampoule was then sealed with a crimp cap. A control ampoule was prepared for each
249 experiment containing only nutrient broth and the same inoculum of bacteria. The ampoule was
250 vortexed briefly before being transferred to a 2277 Thermal Activity Monitor (TAM, TA Instruments
251 Ltd, UK).

252

253 The ampoules were allowed to equilibrate for up to 30 min before being lowered into the measuring
254 position of the TAM (set at 37 °C with an amplifier setting of 1000 µW). Digitam 4.1 software
255 collected heat output data every 10 s for 48 h.

256

257 After calorimetric analysis, ampoules were removed from the TAM and inspected for turbidity. Non-
258 turbid ampoules were vortexed for 10 s then opened and 1 mL of nutrient broth removed to
259 enumerate the bacteria. The sample was centrifuged at 3000 g for 10 min and resuspended in PBS
260 three times in an attempt to remove any metal ions that could affect the growth of the bacteria on
261 agar. The resulting bacterial suspension underwent serial dilution and spread plating on ISA,
262 followed by incubation overnight at 37 °C. Colonies were counted, and the number of viable bacteria
263 in the ampoule calculated.

264

265 **3 Results and Discussion**

266 The manufacture of metal-loaded filaments for 3D printing was achieved with PCL. Five metal loaded
267 PCL filaments were produced with different concentrations: Ag (10% w/w)-PCL, Zn (10% w/w)-PCL,
268 Zn (25% w/w)-PCL, Cu (10% w/w)-PCL and Cu (25% w/w)-PCL (Figure 1). The average filament
269 diameter was 1.77 ± 0.3 mm. The metal compounds and the PCL were dissolved in an appropriate
270 solvent mixture and the solution vacuum-dried to obtain pellets with a homogeneously distribution
271 of the metal compound into the PCL.

272

273 One of the most challenging parts of the process was the determination of a common solvent to
274 dissolve both the metal and polymer. For instance, $\text{CuSO}_4 \cdot 5\text{H}_2\text{O}$ and AgNO_3 were soluble in water
275 while ZnO and PCL were insoluble in water. It was established that a single solvent was not adequate
276 to dissolve both the polymer and any of the metals so ultimately a combination of solvents was used
277 to dissolve PCL and the metals (see Methods for the exact combination for each preparation). This
278 method is cheap, versatile and only requires the selection of suitable solvents, moreover the direct
279 extrusion of the metal compounds and PCL is not recommended since that lead to filaments with a
280 very poor distribution of the metal compounds in the PCL.

281 Two factors were critical in ensuring extrusion produced a filament of consistent diameter. Firstly,
282 the extrusion temperature varied depending on the mixture content and how dry the mixture was.
283 Copper-containing mixtures required a lower extrusion temperature (60 °C) compared with the non-
284 copper-containing mixtures (which were extruded at 75 – 80 °C). This could be due to the lower
285 melting temperature of $\text{CuSO}_4 \cdot 5\text{H}_2\text{O}$ (110 °C) compared with AgNO_3 (212 °C) and ZnO (1975 °C).
286 When the extrusion temperature was lower than required, it led to a thicker filament and/or
287 clogging of the extruder. Higher extrusion temperatures led to the extrusion of filaments that were
288 thin and inconsistent (about 1.35 ± 0.05 mm). Secondly, a regular feeding rate was required to
289 produce a uniform filament diameter.

290 SEM micrographs of the filaments revealed that all the filaments had homogenous and uniform
291 surface and cross section, indicating uniform metal distribution inside the filaments (Figure 2).

292 3D templates for wound dressings were successfully obtained from 3D scanning. The resolution of
293 the 3D scanner was one of the main factors determining the quality of the 3D scans, however,
294 lighting conditions (e.g. direct sunlight) and room temperature did affect the depth of acquisition of
295 the scanner.

296 Ag, Cu and Zn loaded PCL dressings were printed. Figure 3 shows an example of a Cu-PCL printed
297 nose dressing (see Appendix 1 for more examples). All the dressings were flexible, most likely due to
298 the elastomeric properties of PCL. These 3D printed dressings have an advantage over conventional
299 flat dressing in that they can dress anatomically complex areas. This would provide more comfort to
300 the patient and improve adherence. The cytocompatibility of PCL in addition to the possibility of
301 incorporating bioactive or antimicrobial agents means that PCL has the potential to be tailored into
302 an effective wound dressing with appropriate bio-physical properties (e.g. vapour permeability and
303 flexibility) and personalised shape and size. The use of metal ions improves the printing performance
304 of the PCL filaments. In a previous study using PCL filaments loaded with salicylic acid for the
305 treatment of acne, the 3D printer was able to manufacture flat disc/patches but not complex shapes
306 as personal shape devices (Goyanes et al., 2016a).

307 FTIR spectra of plain PCL pellets (before 3D printing) exhibited both absorption bands of the –C–H
308 and C=O functional groups at 2942 cm^{-1} and 1722 cm^{-1} respectively (Figure 4). FTIR analysis of the
309 printed plain PCL, Ag(10%)-PCL, Cu(10%)-PCL, Cu(25%)-PCL, Zn(10%)-PCL and Zn (10%)-PCL showed
310 all absorption bands of the functional groups (–C–H and C=O). In addition, there was no shift in peak
311 positions of the metal-loaded 3D printed samples compared to plain PCL pellets or 3D printed PCL,
312 indicating that there was no chemical bonding between PCL, Ag, Cu or Zn had occurred during
313 extrusion and printing of the dressings.

314 The main limiting factor in printing good dressings was a consistent filament diameter within an
315 acceptable range for the 3D printer. A filament thin in sections resulted in areas of the dressings
316 containing less material than other areas, and thicker filament sections were too difficult for the

317 extruder head to grip. Thus, after various experimentations with slight variations in filament
318 diameters, it was determined that the consistency of the filament diameter (1.69 – 1.77 mm) was
319 more important than the size of the diameter (given that it is within acceptable range of the 3D
320 printer; 1.60 – 1.79 mm).

321 3D printing of wound dressings of good quality requires an understanding of the settings that will
322 ultimately dictate how they would turn out. For dressings printed in this work, these settings were
323 the layer height, number of outer shells and both speed while extruding and travelling. These
324 settings, individually or combined, did directly control the surface finish, density and quality of the
325 final print.

326 Increasing the number of shells (the outer most layers of the print) provided stronger dressings;
327 however, they increased printing time and reduced quality (e.g. 4 shells resulted in substantial
328 reduction of details and inconsistent surface of printed dressings compared to 2 shells). Having too
329 few shells resulted in a weak and fragile print. There needs to be a balance between not having
330 enough or too many shells, and in this case, the default of two outer shells was a good compromise.

331 The resolution of the 3D printed dressing is determined by the layer height. Using a smaller layer
332 height provided a considerable increase in detail and increased printing time. The MakerBot
333 Replicator 2X can print in layer heights between 0.1 mm and 0.3 mm, however it was only possible
334 to obtain good quality prints with 0.1 mm layer heights. One reason for this is because 3D prints
335 made with FDM printers typically have visible ridges between different layers, and a smaller layer
336 height helps to reduce (but not eliminate) them.

337 The printing temperature in addition to both printing and movement speed determine if it is
338 possible to print at all. The extrusion temperature depends on the filament material being used, for
339 instance, plain PCL dressings could be printed with as low as 140 °C. However, when PCL is loaded
340 with metals, it was not possible to print until this temperature was increased to 170 °C. High
341 movement speed while printing or travelling reduced the printing time by making the print-head
342 move faster, but resulted in poorer print quality. On the other hand, slower speed meant that the
343 hot print-head would stay longer above the extruded layers resulting in burnt layers, especially the
344 last layers. The optimal settings found in this case was 50 mm/s for both printing and travelling
345 speeds.

346
347 The DSC thermogram (Figure 5) shows that plain PCL dressing has a melting temperature (T_m) of
348 60.9°C and a glass transition temperature (T_g) of -63.4 °C which agrees with the literature values of
349 PCL pellets (60.0 °C and -60.0 °C respectively) (Hutmacher et al., 2001). All the metal loaded
350 dressings show similar thermal profiles compared with the plain PCL dressing without any
351 degradation at temperatures up to 200 °C. Ag-PCL had the lowest T_m (59.4 °C) while Zn-PCL had the
352 highest (61.8 °C). Ag-PCL dressing decreased the T_m while both Zn-PCL and Cu-PCL dressings
353 increased it slightly, these changes did not have effect on the printability of the filaments.

354 TGA showed no significant mass loss (0.44% to 1.89%), most likely due to loss of residual solvents.
355 Copper-containing dressings (10 and 25% w/w) showed the highest amount of weight loss (1.63%
356 and 1.89% respectively) compared with the other dressings. This could be due to the hygroscopicity
357 of copper sulphate. This might become an issue in the future during storage and transport of the
358 dressings. However, with proper storage conditions and packing this concern can be overcome.

359 Thus it can be concluded that the thermal analysis results confirm that the printed dressings were
360 stable and that the printing and extrusion processes did not affect the properties of PCL. It is

361 important to note that even though the residence time of the formulation in the print head is short
362 (a few seconds), thermally labile formulations may experience some degree of degradation during
363 the printing process (Goyanes et al., 2016a). Hence, DSC analysis may be used to assess the
364 suitability of the formulation for FDM 3D printing (Goyanes et al., 2015a).

365 One of the challenges in antimicrobial research for wound dressings is achieving sustained release of
366 the antimicrobial agent for extended prevention of bacterial infection. The release of Ag, Cu and Zn
367 from PCL dressings to the surrounding environment is shown in Figure 6. During the first 24 h of the
368 experiment, Ag was released very quickly (40.69 µg/mL), but the release rate decreased rapidly in
369 the following 24 h reaching a concentration of 44.53 µg/mL at 48h. From 48 to 72 h the
370 concentration of Ag remained almost constant at 45.85 ± 1.10 µg/mL. The fast release observed in
371 the first 24 h is most likely the release of Ag from the surface of the PCL matrix, and the slower
372 release afterwards is due to the slow diffusion of Ag from the interior of the polymer matrix to the
373 surface before release. The final concentration (44.53 µg/mL) is two folds higher than the minimum
374 inhibitory concentration and minimum bactericidal concentration previously reported for silver
375 against *S. aureus* (22.083 µg/mL) (Said et al. 2014).

376

377 Over the same time period (0 – 72 h) the concentration of Cu and Zn had the same trend but was
378 always much lower compared to Ag. The release rate was highest for 10% Ag-PCL (45.85 µg/mL) and
379 lowest for 10% Zn-PCL (15.87 µg/mL). Both 25% Cu-PCL and 25% Zn-PCL had higher release rate
380 compared to their corresponding 10% dressings. This is due to the fact that the metal content in the
381 25% dressing is higher than the 10% leading to more metal being released. 25% Cu-PCL had higher
382 release rate than 25% Zn-PCL (same applies for the 10% dressings of both metals). Minimum
383 inhibitory concentration for copper against *S. aureus* was reported to be between 3 – 40 µg/ml,
384 being the minimum bactericidal concentration between 7 and 60 µg/ml (Argueta-Figueroa et al.
385 2014). The amount of copper released from the dressings was 17.756 µg/ml (for 10%) and 26.634
386 (for 25%), values which fall in the middle of the reported values. However, the antibacterial efficacy
387 of Zn and Cu is dependent on the concentration of the metal, the initial bacterial concentration, and
388 the strains of bacteria employed in the study.

389 The minimum inhibitory concentrations found in the literature for Zn against *S. aureus* are very
390 variable and not comparable to the test performed in this study. Zn nanoparticles vs *S. aureus*
391 showed a minimum inhibitory concentration determined by agar dilution method of 625 µg/ml
392 (Aleaghil et al. 2016). The highest concentrations obtained were 15.87 µg/ml for 10% and 20.63
393 µg/ml for 25% Zn wound dressings, which are significantly lower than the concentration reported.

394

395 The controlled release of Ag, Cu and Zn from PCL dressings is attributed to the entrapment of the
396 metals into PCL, which acts as a barrier for the release of these metals from the dressing due to the
397 slow water penetration into the PCL matrix. These results confirm that entrapment of metal ions
398 into PCL dressings delays the release of the metals. This is desirable to maintain sufficient release of
399 antimicrobial agent to remain active for the duration of treatment, while preventing high
400 concentrations to be released upon initial application which would prevent adverse events (such as
401 irritation) from high doses. Another advantage of a slower and prolonged release rate of Ag, Zn and
402 Cu in clinical practice is that it would reduce the number of dressing changes, which can be very
403 painful (Meaume et al., 2004).

404

405 These results are in agreement with the solubility of the metals in water (majority constituent of the
406 phosphate buffer testing medium) where Ag has superior solubility properties, followed by Cu then
407 Zn. Ideally, the dissolution testing could have been performed in the same medium used in the

408 antibacterial testing. This could give a better correlation between release profiles of the metals from
409 dressings and antibacterial activity. However, that was not possible as the nutrient broth used for
410 antibacterial testing contains NaCl which led to the precipitation of solid AgCl when Ag-PCL dressing
411 was dissolved in the medium during the initial experiments. Moreover, pH 7.4 of the phosphate
412 buffer resembles the pH at surface of the skin providing closer correlation to the *in-vivo*
413 environment.

414 Isothermal micro-calorimetry (IMC) was used to quantitatively monitor the efficacy of silver, zinc and
415 copper in wound dressings. IMC monitors the rate of heat production (power) in a sample, where
416 the power signal is proportional to the number of viable cells in the sample. This allows for real-time
417 measurement of the growth (or inhibition) of *S. aureus*, without being affected by non-viable cells.
418 This method is not dependent on optical clarity (which can be effected by the presence of the metal
419 ions in the sample), and does not require the organism to be removed from its environment to be
420 sampled (Gaisford et al., 2009; O'Neill et al., 2003). The drawback of IMC is that because heat is
421 absorbed or produced by different events occurring in the sample, could mean that the power signal
422 measured is potentially a combination of several processes. However, a careful experimental design
423 can improve these issues as discussed by S. Gaisford et al. (Gaisford, 2005).

424 The control experiments of *S. aureus* (without any dressing or metals) shows a characteristically
425 complex pattern, exhibiting an exponential growth phase in the first few hours with two distinctive
426 biphasic peaks, during which heat is generated and an increase in power is recorded (Figure 7A). The
427 area under the curve (AUC – total heat output) of the controls is reproducible ($n = 3$) to 3.5%. As
428 discussed by Zaharia et al. (2013), the first exponential phase (0 – 3 h) represents aerobic
429 metabolism where the available oxygen (blue arrow in Figure 7A), dissolved in the medium is utilised
430 (the ampoules are sealed but not completely filled to the top). This is then followed by a change in
431 aerobic metabolism (3 – 10 h) using diffused oxygen from the head space of the ampoule (red arrow
432 in Figure 7A). The last peak of the thermogram represents anaerobic metabolism of the organism
433 using any remaining carbon sources that the organism is able to metabolise (green arrow in Figure
434 7A) (Zaharia et al., 2013). The exhaustion of nutrients, pH drift and the appearance of toxic
435 metabolites consequently stopping the organism from growing anymore. This resulted in the power
436 signal to return to baseline (zero) and hence decided the 48 hour duration of the experiment.

437
438 In the presence of plain 3D PCL dressings (i.e. the dressings with no antimicrobial metal agent), PCL
439 showed no effect on the initial aerobic phase and the overall growth is very similar to that of the
440 control (Figure 7B). There was very slight variation in the second growth phase which was attributed
441 to microorganism cells becoming entrapped within the PCL dressing. Therefore, diffusion of medium
442 to those trapped cells and metabolites from those microorganisms to the medium will be different
443 compared to those present in the surrounding medium only. Thus, it can be concluded that PCL does
444 not have any intrinsic antimicrobial properties, and increasing amounts of PCL does not affect the
445 growth of *S. aureus*.

446
447 The shape of the growth curve is significantly different in the presence of 10% (w/w) Ag-PCL dressing
448 (Figure 7C). Use of 10 mg of Ag-PCL dressing delayed the growth by *ca.* 16 h, and inhibition of growth
449 was observed when larger masses (20, 30 and 40 mg) were used when compared to the control.
450 Viable counts at the end of each experiment (Table 1) confirmed a bactericidal effect on the
451 bacteria, with a three log reduction in bacteria compared to the inoculum. These results indicate
452 that silver dressing is effective at inhibiting the growth of *S. aureus* via a bactericidal mechanism, and
453 that increasing amount of silver causes a more potent inhibition.

454

455
456
457
458
459
460
461
462
463
464
465
466

Table 1. Viable cell counts after the IMC study

Formulation		10% Ag - PCL			
Mass of the dressing	Control (0g)	10 mg	20 mg	30 mg	40 mg
Viable cells	140,333	105	20	0	0
Formulation		10% Cu - PCL			
Mass of the dressing	Control (0g)	25 mg	50 mg	75 mg	100 mg
Viable cells	121,667	120,311	95,038	56,664	51,682
Formulation		25% Cu - PCL			
Mass of the dressing	Control (0g)	25 mg	50 mg	75 mg	100 mg
Viable cells	120,660	14,738	1,202	220	48
Formulation		10% Zn - PCL			
Mass of the dressing	Control (0g)	25 mg	50 mg	75 mg	100 mg
Viable cells	119,333	117,855	117,439	111,538	89,795
Formulation		25% Zn - PCL			
Mass of the dressing	Control (0g)	10 mg	20 mg	30 mg	40 mg
Viable cells	119,916	84,764	81,297	71,859	68,315

467
468
469
470
471
472
473
474
475
476
477
478
479
480
481

Figure 7D shows the corresponding growth curves for *S. aureus* in the presence of increasing masses of 10% (w/w) Cu-PCL. All the samples (10 – 40 mg) showed no inhibition of the microorganism. This indicates that at this concentration Cu is ineffective at inhibiting the growth of *S. aureus* after 48 h, due to a slow release rate or the concentration of Cu is not sufficient. Hence, 25% (w/w) Cu-PCL was tested to determine if there is any improvement with higher concentrations of Cu (Figure 7E). Several differences from the control are apparent, but the interpretation of these data is difficult. There is an absence of any of the characteristic growth peaks of *S. aureus*, with high-power peaks at the beginning with an immediate sharp decline in power instead. There was no growth in any of the samples, which was confirmed by the non-turbidity of all the samples after the TAM experiments. In addition, viable counts revealed that a 25 mg dressing showed a two log reduction in viable bacteria (while higher masses of the dressing had stronger inhibition) at the end of the TAM experiment compared to the initial inoculum (Table 1). This suggests that Cu is effective at inhibiting the growth of *S. aureus*, although higher concentrations are required compared to silver. In efforts to explain

482 the unusually high peaks at the start of the growth curves are due to Cu, the bacteria or an
483 interaction between any of dressings' content's and that of the medium, copper sulphate powder
484 only (without any bacteria or PCL) was tested exactly as the Cu-PCL dressing in water and broth. As
485 can be seen in Figure 7F, both curves show a similar pattern to that of the 25% (w/w) Cu-PCL. This
486 confirms that these peaks are due to copper sulphate powder and are not due to any interaction
487 between the dressing content, bacteria or the medium.

488

489 Both 25 and 50 mg of 10% (w/w) Zn-PCL dressing showed no effect on the growth of *S. aureus* after
490 72 h (Figure 7G). While 75 mg and 100 mg of the dressing showed a small reduction in the intensity
491 of the growth peaks, and a minor delay of the growth. These results suggest that at these
492 concentrations Zn is ineffective at inhibiting the growth of *S. aureus*, as confirmed by cell counting
493 (Table 1).

494 The results with 25% (w/w) Zn-PCL show stronger inhibition compared to the 10% (w/w) Zn-PCL
495 dressing (Figure 7H). Both 10 and 20 mg of 25% Zn-PCL showed similar inhibition, which was weaker
496 compared to 30 and 40 mg of the dressing. In addition, there was a time delay of the growth (34 –
497 82 min). These results suggest that increasing the concentration of Zn to 25% (w/w) increases the
498 inhibition, however, it is not as effective as Ag or Cu. This is most likely due to a weaker bactericidal
499 efficacy and lower release rate of Zn compared to Ag and Cu. Consequently, higher amounts of Zn
500 may be required to be incorporated into the dressing to compensate for the low release rate and
501 efficacy to achieve similar inhibition of Cu or Ag. This may present certain difficulties during
502 formulation and an increase in cost. However, this may not be required as Zn can be incorporated
503 into the dressing to benefit from its healing properties (especially in patients with zinc deficiency), in
504 addition to the weaker antimicrobial efficacy.

505 It is important to make some clarifications regarding the nature of the assay method (IMC) used in
506 this work. Any *in vitro* method will differ from the *in vivo* event, and the relevancy of these
507 differences will depend on how the data is used. In this case, the *in vivo* environment is extremely
508 difficult to reproduce. In a wound environment, bacteria can grow as biofilms or micro-colonies
509 rather than planktonic cultures which can influence the susceptibility of the microorganism to an
510 antibacterial agent (James et al., 2008). For instance, it has been suggested that the bactericidal
511 concentration of silver required to eradicate biofilms of *Pseudomonas aeruginosa* is 10 to 100 fold
512 higher than what is required to eradicate planktonic bacteria (Bjarnsholt et al., 2007). This would
513 suggest that the concentrations used in this work might need to be increased to eradicate biofilms,
514 since in the experiments reported here, the organism is growing in planktonic culture. In addition,
515 the antimicrobial effect of metal ions is known to be strain dependent (Ruparelia et al., 2008). It is
516 important to note that the metal release would be lower in skin versus suspending solution,
517 although the release could be promoted increasing the metal loading in the filaments, so in the 3D
518 printed wound dressings as shown in the ICP data. It is already reported that increasing the drug
519 loading in 3D printed formulations increased drug release since there is less matrix compound (in
520 this case PCL) avoiding the release of the active compounds (Goyanes et al., 2016b). The main aim of
521 the microbiology experiments was to evaluate the efficacy of the metal loaded PCL wound dressings
522 against a known skin pathogen (*S. aureus*), and to gain insights on how 3D printing might influence
523 the outcome.

524 Since optimal moisture content maintains the vitality of tissue and promotes wound healing,
525 theoretically, it would be possible to modify the thickness of the wounds dressings or to create
526 regions with small gaps between the layers to modify the vapour permeability.

527

528 **4 Conclusion**

529 The results clearly demonstrate the utility of hot melt extrusion as a novel method to incorporate
530 antimicrobial Ag, Cu and Zn into polycaprolactone filaments that allow the 3D printing of
531 personalised wound dressings. 3D printed dressings demonstrated a clear advantage over
532 conventional flat dressings as they are anatomically adaptable. This method takes advantage of 3D
533 scanning to create 3D models of body parts which are then 3D printed in a personalised therapy. Ag-
534 PCL and Cu-PCL dressings showed the most bactericidal properties against *S. aureus* which is a
535 common bacterium to causes skin infections. This study therefore demonstrates a simple method to
536 produce customizable wound dressings that can be tailored to individual patients in regards to
537 shape, size and antimicrobial agents.

538

539 **5 Acknowledgment**

540 The authors wish to thank Professor John McArthur (Earth Sciences, UCL) for his advice and
541 assistance with the ICP-AES machine.

542

543 **6 References**

544

545 Bjarnsholt, T., Kirketerp-Møller, K., Kristiansen, S., Phipps, R., Nielsen, A.K., Jensen, P.Ø., Højby, N.,
546 Givskov, M., 2007. Silver against *Pseudomonas aeruginosa* biofilms. *Apmis* 115, 921-928.

547 Boateng, J., Catanzano, O., 2015. Advanced Therapeutic Dressings for Effective Wound Healing--A
548 Review. *J. Pharm. Sci.* 104, 3653-3680.

549 Boateng, J.S., Matthews, K.H., Stevens, H.N., Eccleston, G.M., 2008. Wound healing dressings and
550 drug delivery systems: a review. *J. Pharm. Sci.* 97, 2892-2923.

551 Borkow, G., Gabbay, J., 2005. Copper as a biocidal tool. *Curr. Med. Chem.* 12, 2163-2175.

552 Chopra, I., 2007. The increasing use of silver-based products as antimicrobial agents: a useful
553 development or a cause for concern? *J. Antimicrob. Chemother.* 59, 587-590.

554 Fielding, G.A., Bandyopadhyay, A., Bose, S., 2012. Effects of silica and zinc oxide doping on
555 mechanical and biological properties of 3D printed tricalcium phosphate tissue engineering
556 scaffolds. *Dent. Mater.* 28, 113-122.

557 Fong, J., Wood, F., 2006. Nanocrystalline silver dressings in wound management: a review. *Int. J.*
558 *Nanomedicine* 1, 441.

559 Freiberg, S., Zhu, X., 2004. Polymer microspheres for controlled drug release. *Int. J. Pharm.* 282, 1-
560 18.

561 Gabbay, J., Borkow, G., Mishal, J., Magen, E., Zatcoff, R., Shemer-Avni, Y., 2006. Copper oxide
562 impregnated textiles with potent biocidal activities. *J. Ind. Text* 35, 323-335.

563 Gaisford, S., 2005. Stability assessment of pharmaceuticals and biopharmaceuticals by isothermal
564 calorimetry. *Curr. Pharm. Biotechnol* 6, 181-191.

565 Gaisford, S., Beezer, A.E., Bishop, A.H., Walker, M., Parsons, D., 2009. An in vitro method for the
566 quantitative determination of the antimicrobial efficacy of silver-containing wound dressings. *Int. J.*
567 *Pharm.* 366, 111-116.

568 Goyanes, A., Buanz, A.B., Basit, A.W., Gaisford, S., 2014. Fused-filament 3D printing (3DP) for
569 fabrication of tablets. *Int. J. Pharm.* 476, 88-92.

570 Goyanes, A., Buanz, A.B., Hatton, G.B., Gaisford, S., Basit, A.W., 2015a. 3D printing of modified-
571 release aminosaliclylate (4-ASA and 5-ASA) tablets. *Eur. J. Pharm. Biopharm.* 89, 157-162.

572 Goyanes, A., Det-Amornrat, U., Wang, J., Basit, A.W., Gaisford, S., 2016a. 3D scanning and 3D
573 printing as innovative technologies for fabricating personalized topical drug delivery systems. *J.*
574 *Control. Release.* 234, 41-48.

575 Goyanes, A., Kobayashi, M., Martinez-Pacheco, R., Gaisford, S., Basit, A.W., 2016b. Fused-filament
576 3D printing of drug products: Microstructure analysis and drug release characteristics of PVA-based
577 caplets. *Int. J. Pharm.* 514, 290-295.

578 Goyanes, A., Wang, J., Buanz, A., Martinez-Pacheco, R., Telford, R., Gaisford, S., Basit, A.W., 2015b.
579 3D Printing of Medicines: Engineering Novel Oral Devices with Unique Design and Drug Release
580 Characteristics. *Mol. Pharm.* 12, 4077-4084.

581 Huh, A.J., Kwon, Y.J., 2011. "Nanoantibiotics": A new paradigm for treating infectious diseases using
582 nanomaterials in the antibiotics resistant era. *J. Control. Release.* 156, 128-145.

583 Hutmacher, D.W., Schantz, T., Zein, I., Ng, K.W., Teoh, S.H., Tan, K.C., 2001. Mechanical properties
584 and cell cultural response of polycaprolactone scaffolds designed and fabricated via fused deposition
585 modeling. *J. Biomed. Mater. Res.* 55, 203-216.

586 Jain, J., Arora, S., Rajwade, J.M., Omay, P., Khandelwal, S., Paknikar, K.M., 2009. Silver nanoparticles
587 in therapeutics: development of an antimicrobial gel formulation for topical use. *Mol. Pharm.* 6,
588 1388-1401.

589 James, G.A., Swogger, E., Wolcott, R., Secor, P., Sestrich, J., Costerton, J.W., Stewart, P.S., 2008.
590 Biofilms in chronic wounds. *Wound Repair Regen.* 16, 37-44.

591 Kamath, M.S., Ahmed, S.S., Dhanasekaran, M., Santosh, S.W., 2014. Polycaprolactone scaffold
592 engineered for sustained release of resveratrol: therapeutic enhancement in bone tissue
593 engineering. *Int. J. Nanomedicine* 9, 183-195.

594 Koch, M., 2012. 3D scanner - Unabridged Guide. Emereo Publishing.

595 Kweon, H., Yoo, M.K., Park, I.K., Kim, T.H., Lee, H.C., Lee, H.-S., Oh, J.-S., Akaike, T., Cho, C.-S., 2003. A
596 novel degradable polycaprolactone networks for tissue engineering. *Biomaterials.* 24, 801-808.

597 Landis, S.J.M.D.F., 2008. Chronic Wound Infection and Antimicrobial Use. *Adv. Skin Wound Care* 21,
598 531-540.

599 Lansdown, A.B., Mirastschijski, U., Stubbs, N., Scanlon, E., Agren, M.S., 2007. Zinc in wound healing:
600 theoretical, experimental, and clinical aspects. *Wound Repair Regen.* 15, 2-16.

601 Lemire, J.A., Harrison, J.J., Turner, R.J., 2013. Antimicrobial activity of metals: mechanisms, molecular
602 targets and applications. *Nat. Rev. Micro.* 11, 371-384.

603 Li, X., Cui, R., Sun, L., Aifantis, K.E., Fan, Y., Feng, Q., Cui, F., Watari, F., 2014. 3D-Printed Biopolymers
604 for Tissue Engineering Application. *Int. J. Polym. Sci.* 2014.

605 Liu, Y., He, L., Mustapha, A., Li, H., Hu, Z.Q., Lin, M., 2009. Antibacterial activities of zinc oxide
606 nanoparticles against *Escherichia coli* O157:H7. *J. Appl. Microbiol.* 107, 1193-1201.

607 Meaume, S., Teot, L., Lazareth, I., Martini, J., Bohbot, S., 2004. Importance of pain reduction through
608 dressing selection in routine wound management: the MAPP study. *J. Wound Care* 13, 409-414.

609 Melocchi, A., Parietti, F., Loreti, G., Maroni, A., Gazzaniga, A., Zema, L., 2015. 3D printing by fused
610 deposition modeling (FDM) of a swellable/erodible capsular device for oral pulsatile release of drugs.
611 *J. Drug Deliv. Sci. Tec.* 30, 360-367.

612 Ng, K.W., Achuth, H.N., Mochhala, S., Lim, T.C., Hutmacher, D.W., 2007. In vivo evaluation of an
613 ultra-thin polycaprolactone film as a wound dressing. *J. Biomater. Sci. Polym. Ed.* 18, 925-938.

614 O'Neill, M.A.A., Vine, G.J., Beezer, A.E., Bishop, A.H., Hadgraft, J., Labetoulle, C., Walker, M., Bowler,
615 P.G., 2003. Antimicrobial properties of silver-containing wound dressings: a microcalorimetric study.
616 *Int. J. Pharm.* 263, 61-68.

617 Pietrzak, K., Isreb, A., Alhnan, M.A., 2015. A flexible-dose dispenser for immediate and extended
618 release 3D printed tablets. *Eur. J. Pharm. Biopharm.* 96, 380-387.

619 Ruparelia, J.P., Chatterjee, A.K., Duttagupta, S.P., Mukherji, S., 2008. Strain specificity in
620 antimicrobial activity of silver and copper nanoparticles. *Acta Biomater.* 4, 707-716.

621 Salgado, C.L., Sanchez, E., Mano, J., Moraes, A., 2012. Characterization of chitosan and
622 polycaprolactone membranes designed for wound repair application. *J. Mater. Sci.* 47, 659-667.

623 Siddiqui, A.R., Bernstein, J.M., 2010. Chronic wound infection: facts and controversies. *Clin.*
624 *Dermatol.* 28, 519-526.

625 Tenaud, I., Saiagh, I., Dreno, B., 2009. Addition of zinc and manganese to a biological dressing. *J.*
626 *Dermatolog. Treat.* 20, 91-94.

627 Yu, D.G., Zhu, L.M., Branford-White, C.J., Yang, X.L., 2008. Three-dimensional printing in
628 pharmaceuticals: Promises and problems. *J. Pharm. Sci.* 97, 3666-3690.

629 Zaharia, D.C., Muntean, A.A., Popa, M.G., Steriade, A.T., Balint, O., Micut, R., Iftene, C., Tofolean, I.,
630 Popa, V.T., Baicus, C., Bogdan, M.A., Popa, M.I., 2013. Comparative analysis of *Staphylococcus*
631 *aureus* and *Escherichia coli* microcalorimetric growth. *BMC microbiology* 13, 171.

632 Zahedi, P., Rezaeian, I., Ranaei-Siadat, S.O., Jafari, S.H., Supaphol, P., 2010. A review on wound
633 dressings with an emphasis on electrospun nanofibrous polymeric bandages. *Polymer. Adv. Tech.* 21,
634 77-95.

635

636

637

638

639 **Figure Captions**

640 **Figure 1.** Filaments loaded with metals produced, from left to right: plain PCL, Ag (10% w/w)-PCL, Zn
641 (10% w/w)-PCL, Zn (25% w/w)-PCL, Cu (10% w/w)-PCL and Cu (25% w/w)-PCL.

642 **Figure 2.** SEM images of: (A) plain PCL, (B) Ag (10% w/w)-PCL, (C) Cu (10% w/w)-PCL, (D) Cu (25%
643 w/w)-PCL, (E) Zn (10% w/w)-PCL and (F) Zn (25% w/w)-PCL.

644 **Figure 3.** 3D scan model of a nose (left) and the printed wound dressing of this model with Cu-PCL
645 (right).

646 **Figure 4.** FTIR spectra of the 3D printed dressings.

647 **Figure 5.** DSC analysis of indicated PCL wound dressings. Exothermic up.

648 **Figure 6.** Dissolution profiles of Ag (10% w/w)-PCL, Cu (10% w/w)-PCL, Cu (25% w/w)-PCL, Zn (10%
649 w/w)-PCL and Zn (25% w/w)-PCL in phosphate buffer (pH 7.4).

650 **Figure 7.** Growth of *S. aureus* by showing the power generated of bacterial cells vs. time in the
651 presence of increasing amount of dressing containing: (A) control experiments with no PCL or any
652 metal ions, (B) plain PCL, (C) Ag (10% w/w)-PCL, (D) Cu (10% w/w)-PCL, (E) Cu (25% w/w)-PCL, (F)
653 control experiment of plain CuSO₄ powder in broth and water without any PCL or bacteria, (G) Zn
654 (10% w/w)-PCL and (H) Zn (25% w/w)-PCL. All experiments were performed at 37 °C over 48 h.

655

656

657 Figure 1

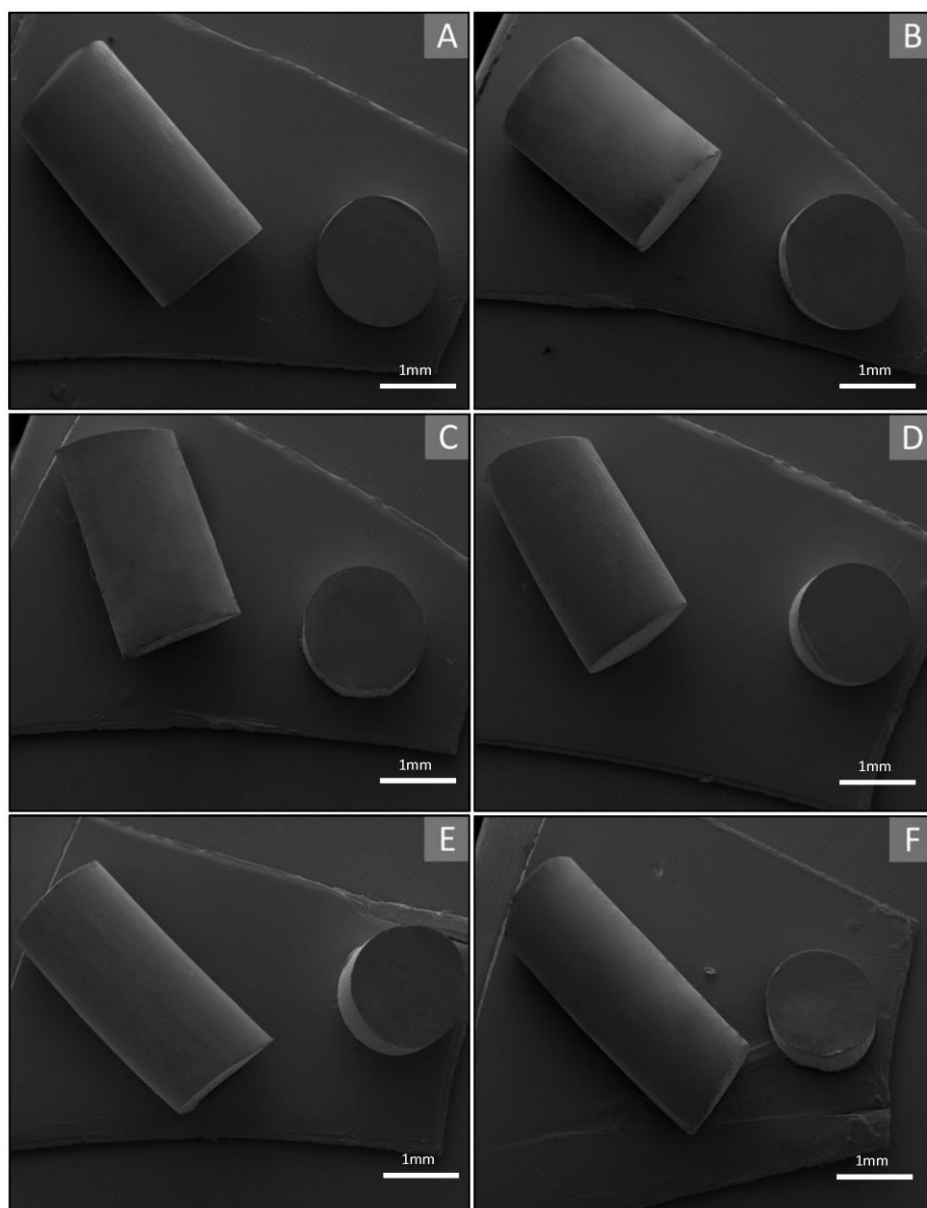
658

659

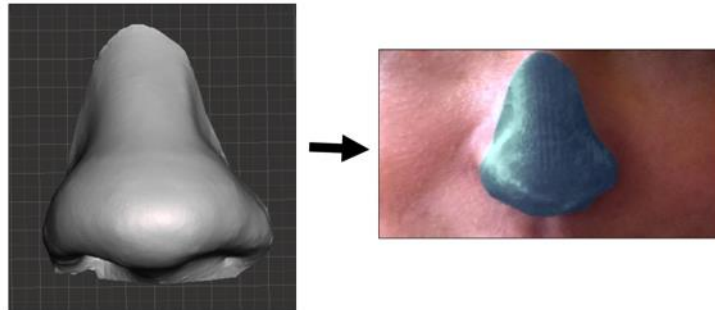


660

661



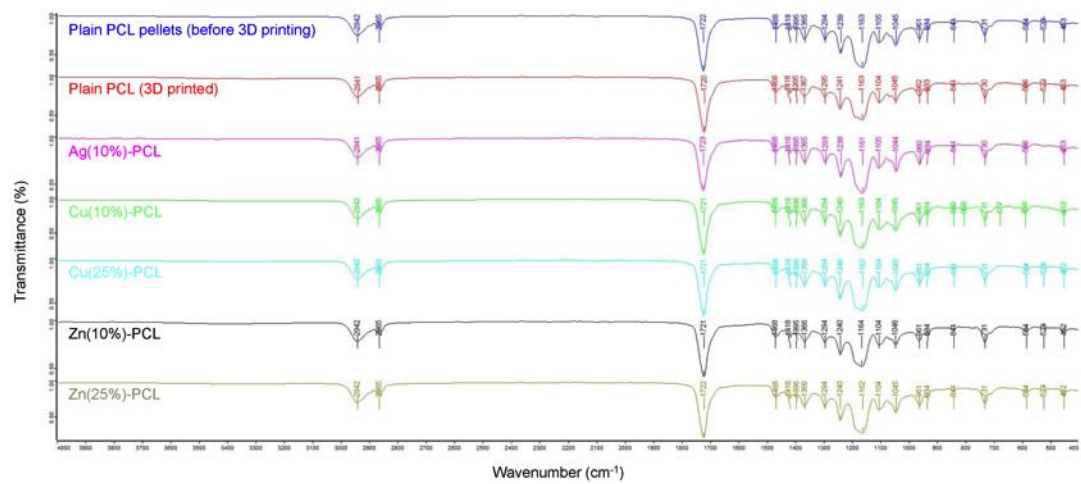
665 **Figure 3**



666

667

668 **Figure 4**

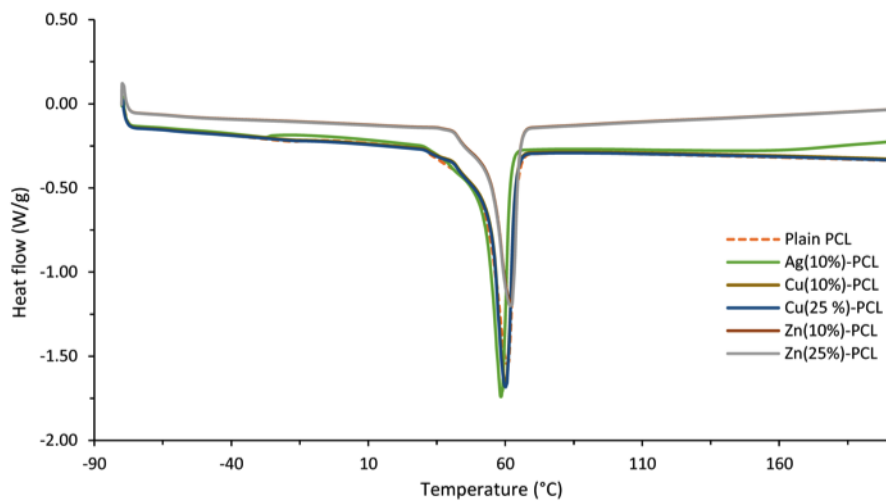


669

670

671

672 **Figure 5**

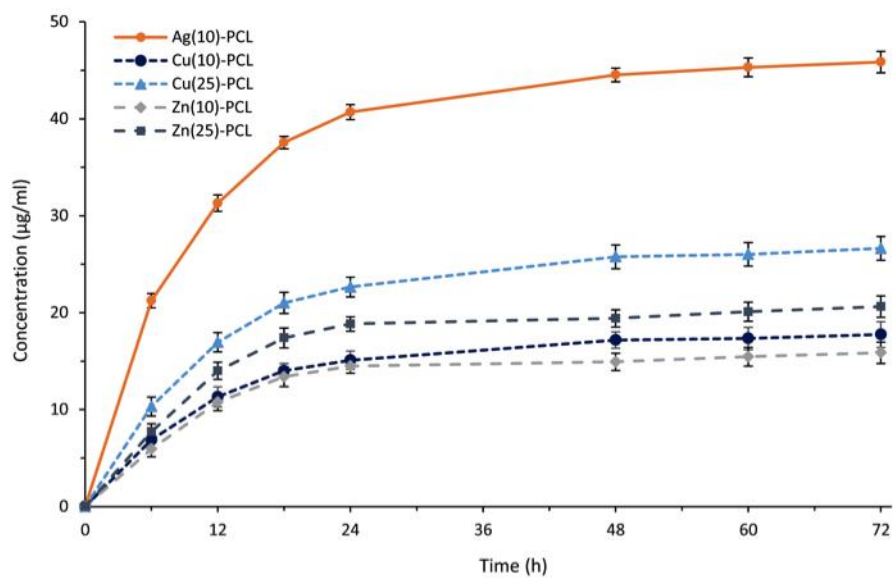


673

674

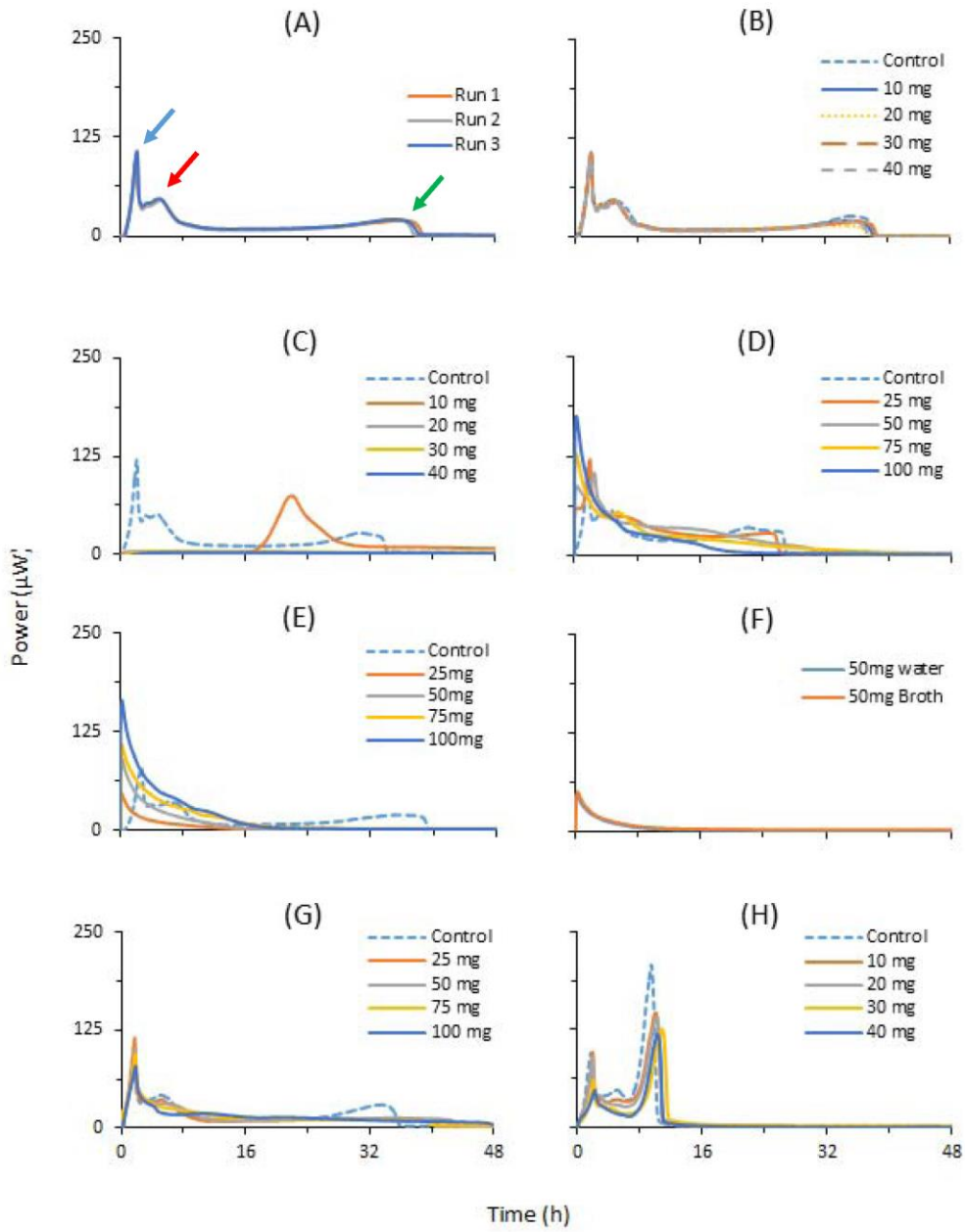
675 **Figure 6**

676



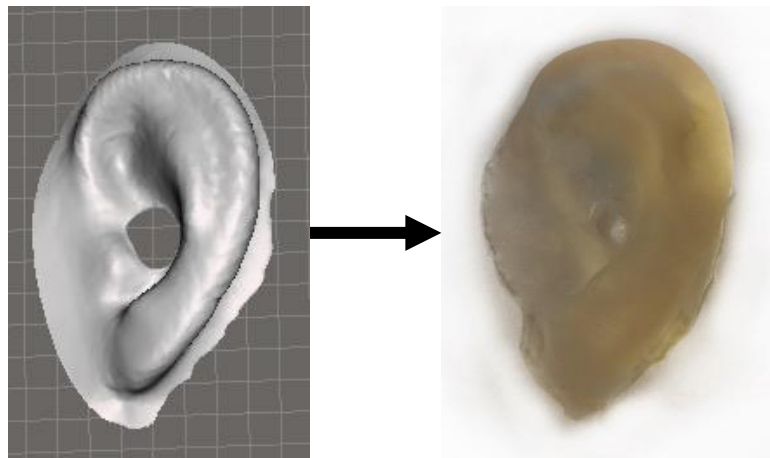
677

678



682 **Appendix 1**

683



684

685

Figure 8. 3D scan model of an ear (left) and the printed wound dressing of this model with Ag-PCL (right).